


STIM1 knock-down decreases the affinity of obinutuzumab for CD20 by altering CD20 localization to Triton-soluble membrane

W. Heo,* N. Jin,* M. S. Park,*
H.-Y. Kim,* S. M. Yoon,[†] J. Lee[†] and
J. Y. Kim *

*Department of Pharmacology and Brain,
Korea 21 Project for Medical Science, Yonsei
University College of Medicine, Seoul, and
[†]College of Pharmacy, Yonsei Institute of
Pharmaceutical Sciences, Yonsei University,
Incheon, Korea

Accepted for publication 11 February 2020
Correspondence: J. Lee, College of Pharmacy,
Yonsei Institute of Pharmaceutical Sciences,
Yonsei University, Incheon 21983, Republic of
Korea.

E-mail: jinulee@yonsei.ac.kr and

J. Y. Kim, Department of Pharmacology and
Brain Korea 21 Project for Medical Science,
Yonsei University College of Medicine, Seoul
03722, Republic of Korea.

E-mail: jooyoungkim@yuhs.ac

Introduction

In recent years there has been considerable progress in the development of anti-cancer strategies using antibodies. The success of anti-CD20 antibody therapy, initiated with rituximab, not only led to the development of bio-better antibodies, but also to the success of various anti-cancer drugs [1]. Anti-CD20 antibodies have been shown to be useful for chemotherapy-free anti-cancer strategies [2].

Obinutuzumab is a Type II humanized anti-CD20 monoclonal antibody that shows enhanced antibody-dependent cellular cytotoxicity (ADCC) via glyco-engineering [3,4]. This drug shows efficacy for treating rituximab-resistant chronic lymphocytic leukaemia [5,6] and has become the first-line treatment for follicular lymphoma [7]. Major cell death caused by obinutuzumab is mediated by ADCC but not complement-dependent cytotoxicity; in particular, direct cell

Summary

Obinutuzumab is thought to exert its effects through its high antibody-dependent cellular cytotoxicity (ADCC) via glyco-engineering of the Fc region. In addition, obinutuzumab causes direct binding-induced cell death (DCD) only by specifically binding to its target CD20, a Ca²⁺ channel. However, the specific features of CD20 related to obinutuzumab binding-induction of cell death are not clearly understood. In this study, we evaluated the relationship between the Ca²⁺ channel features of CD20 as a store-operated Ca²⁺ channel (SOC) and obinutuzumab binding-induced cell death. Ca²⁺ channel function and biochemical analysis revealed that CD20 is an Orai1- and stromal interaction molecule (STIM1)-dependent Ca²⁺ pore. However, binding of obinutuzumab on CD20 did not have any effect on Ca²⁺ influx activity of CD20; the direct cell death rate mediated by obinutuzumab binding was almost equivalent with or without the extracellular Ca²⁺ condition. Given the apparent interaction between STIM1 and CD20, we observed Triton-X solubilized obinutuzumab-bound CD20 accompanied by STIM1. Subsequently, obinutuzumab binding and cell death were decreased by STIM1 knock-down in Ramos B cells. Thus, STIM1 directly contributes to cell death by increasing the affinity of cells for obinutuzumab by transferring CD20 to the Triton-soluble membrane region.

Keywords: Ca²⁺, CD20, direct binding-induced cell death, obinutuzumab, raft, STIM1

death caused by binding without a cross-linking antibody is a typical feature observed in lysosomal membrane permeabilization and non-apoptotic cell death [3,8,9].

CD20 is a successful target antigen used in immunotherapy for haematological malignancies [10–12]. CD20 is a raft-localized protein with a raft-localizing region in its cytoplasmic C-terminal tail near the fourth transmembrane domain [13,14], and is characterized by a Ca²⁺ channel that increases Ca²⁺ influx under channel over-expression [12] and Ca²⁺ store-depleted conditions [15,16]. The raft localization and Ca²⁺ influx activity of CD20 are targets for immunotherapy and the cause of resistance to the most widely used anti-CD20 antibody, rituximab [17]. Ca²⁺ influx through CD20 induced by rituximab is well understood [16,18,19]; Ca²⁺ influx is activated by rituximab binding to CD20, which is induced by the release of stored

Ca²⁺ via B cell receptor activation [19,20]. Additionally, Ca²⁺ influx of CD20 is related to resistance to rituximab treatment [21]. The relationship between Ca²⁺ and obinutuzumab binding is not clearly understood. The fact that cell death occurs only by obinutuzumab binding leads us to expect that excessive Ca²⁺ influx through CD20 is the underlying cell death mechanism. However, reports of intracellular calcium responses after binding of obinutuzumab remain controversial, and there are no reports supporting the hypothesis that Ca²⁺ influx is a key cell death mechanism. Therefore, in-depth understanding of the CD20 channel features, its exact biological role and interactions with obinutuzumab binding and cell death are essential to unveil the pharmacological mechanism of obinutuzumab.

Rituximab binding to CD20 causes CD20 aggregation in the raft region, which is one of the typical characteristics of Type I categorized CD20 antibodies [16]. This enhances the efficient establishment of a mega pore by activating the complement cascade which, in turn, causes complement-dependent cytotoxicity [1,22,23]. In contrast, Type II antibodies such as obinutuzumab do not cause CD20 aggregation in the raft region, and thus show low complement-dependent cell death and instead exhibit high ADCC [3,24]. The epitope region is bound by rituximab and obinutuzumab overlap [25]; however, only obinutuzumab causes binding-induced cell death [3,8,9]. Structural analysis has revealed that the binding mode and plasma membrane localization of rituximab and obinutuzumab differ [25,26]. Obinutuzumab does not bind to the CD20 in raft and is dissolved in Triton, while rituximab binds to raft-located CD20 and does not dissolve in Triton [3,23]. Thus, obinutuzumab and rituximab combine differently with CD20 in different locations [23,25–27].

Stromal interaction molecule (STIM1) was first identified as a protein with increased expression in B cell lymphocytes and cancer [13,14]. In 2006, STIM1 was found as the only regulatory switch of store-operated Ca²⁺ channels such as Orai1, a representative store-operated channel (SOC) [28–30]. STIM1 forms an endoplasmic reticulum–plasma membrane contact site [29], which shows different characteristics from other plasma membrane regions [31,32]. This is where ion channels such as Orai1 form puncta in the membrane, which is more fluid than the neighbouring region, but the puncta form a rigid membrane to anchor the membrane protein [33]. The contribution of STIM1 and Orai1 to rituximab-induced Ca²⁺ influx through CD20 has been reported [16,34]. However, their roles in obinutuzumab-related events remain unclear, particularly the role of STIM1 in binding-induced cell death. In this study, we evaluated the relationship between the characteristics of CD20 as a store-operated Ca²⁺ channel and obinutuzumab binding-induced cell death.

Materials and methods

Cells and short interfering RNA (siRNA) transfection

The human B lymphoma Ramos cell line was purchased from the Korean Cell Line Bank (Seoul, Korea). Cells were maintained in RPMI-1640 media supplemented with 10% fetal calf serum and 1% penicillin/streptomycin at 37°C, 5% CO₂. siRNA transfection into Ramos cells was mediated using a Neon transfection instrument (Invitrogen, Carlsbad, CA, USA) with appropriate reagents. The cells (1 × 10⁶) were washed twice with phosphate-buffered saline (PBS) and then resuspended in 10 µl of T reagent and mixed with 1 µl of 100 nM siRNA for STIM1. The final volume of 11 µl was suctioned with a 10-µl Neon tip and pulsed once at a width of 40 and voltage of 1100 for electric shock. The overall cell survival rate was 70%. The cells were incubated in prewarmed RPMI media for 72 h and reduced STIM1 expression was confirmed by Western blot analysis with an anti-STIM1 antibody (610954; BD Transduction Laboratories™, San Jose, CA, USA). Myc-STIM1 expressed in the human kidney embryo (HEK) cell lysate were used as the positive control for STIM1 protein and an anti-β-actin antibody (Santa Cruz Biotechnology, Dallas, TX, USA) was used as a protein loading control. The HEK 293T cell line was maintained in Dulbecco's modified Eagle's medium (DMEM) media supplemented with 10% fetal bovine serum (FBS) and 1% penicillin/streptomycin at 37°C, 5%. To express CD20 or STIM1 in HEK cells, lipofectamine 2000 reagent was used according to the manufacturer's protocol.

Reagents and solutions

Cell cultures, DMEM (11995-065), RPMI-1640 (11875-093), FBS (26140-079) and penicillin–streptomycin (15140-122) were from GIBCO (Grand Island, NY, USA). Trypsin-ethylenediamine tetraacetic acid (EDTA) 0.05% solution (25300-062) was also from GIBCO. For immunoblotting, NaCl (S7653), Triton X-100 (T8787) and glycerol (G5516) were obtained from Sigma Aldrich (St Louis, MO, USA). EDTA (15694) was from USB Corporation (Cleveland, OH, USA). Tris Ultrapure (T1501) was from Duchefa (Haarlem, the Netherlands). Complete proteinase inhibitor was from Roche Applied Science (Mannheim, Germany). HCl (084-05425) and NaOH (196-05375) were from Wako (Osaka, Japan). The BCA Protein Assay Kit (23227) was from Pierce (Rockford, IL, USA). The ×5 tricine-sodium dodecyl sulphate (SDS) sample buffer (KTR020-5) and premade 4–12% gradient SDS-polyacrylamide gel electrophoresis (PAGE) gels (KG5012) were from KOMA Biotech (Seoul, Korea). Horseradish peroxidase (HRP)-conjugated anti-human IgG (109-035-003) was from Jackson Laboratories (West Grove, PA, USA). For immunocytochemistry, 4% paraformaldehyde (19943), bovine serum

albumin (BSA) (10857; Affymetrix, Santa Clara, CA, USA) horse serum (16050-122, GIBCO), gelatine (G1890), Na₃N (S2002) and PBS (P5493; Sigma Aldrich) were used. As fluorescent dyes, FITC-conjugated goat anti-human IgG antibody (ab81051; Abcam, Cambridge, UK) and Alexa Fluor-568-conjugated anti-mouse IgG antibody (A11004; Invitrogen, Carlsbad, CA, USA) were used.

Generation of rituximab- and obinutuzumab-producing Chinese hamster ovary (CHO)-K1 and CHO-GE cells

To produce the rituximab and obinutuzumab in CHO cells, the DNA sequence of each monoclonal antibody (mAb) was determined from the patent document (rituximab, Sequence 3 from patent US 6897044 heavy chain, Sequence 1 from patent US 6897044 light chain; obinutuzumab, patent number US20050123546). Each light- and heavy-chain DNA sequence was synthesized by Bioneer (Daejeon, Korea) and inserted into the pLenti6 viral vector. To generate cells stably expressing rituximab and obinutuzumab, we produced lentiviruses expressing the heavy or light chain of the two antibodies. CHO-rituximab and CHO-obinutuzumab cells were generated by co-transduction of CHO-K1 cells (ATCC, Manassas, VA, USA) with the same titres of heavy- and light-chain viruses followed by double selection in growth medium containing 10 µg/ml puromycin (Sigma) and 10 µg/ml blasticidin S (Sigma Aldrich) for 1 week. To prepare hyper glycol-engineering CHO-K1 (CHO-GE) cells, LVX-GNT-Hygro and LVX-MAN2A-Bleo viruses were transduced and selected with 500 µg/ml of hygromycin (AG Scientific, San Diego, CA, USA) and 100 µg/ml of zeocin (Invitrogen) for 1 week. The resulting CHO-GE cells were used to produce glycol-engineered rituximab and obinutuzumab by transduction with lentiviruses expressing the heavy and light chains of rituximab and obinutuzumab and selected with 10 µg/ml puromycin and 10 µg/ml blasticidin S.

Purification of mAbs

Aldrich PBS and refreshed with EX-CELL[®] CD CHO serum-free media (Sigma Aldrich) containing 1 mM sodium butyrate. Conditioned media containing mAbs were obtained by further incubation for 10 days at 30°C in 5% CO₂/95% air. Antibodies were purified by affinity chromatography using protein A-Sepharose beads (GE Healthcare Life Sciences, Chicago, IL, USA). Buffer changes and protein concentration were conducted by ultrafiltration with Amicon[®] Ultra-2 filters (Millipore, Billerica, MA, USA) before filter-sterilization and storage. The protein characteristics of the antibodies were analysed by SDS-PAGE and Coomassie blue staining. Each antibody concentration was indirectly measured by subtraction according to the relative band intensity of BSA as standard.

Measurement of binding-induced direct cell death

To measure direct cell death, 1×10^5 cells/well Ramos cells were resuspended in 100 µl of serum-free RPMI media or RPMI media containing 1 mM EGTA, after which different concentrations of antibody (0.3, 1, 3, 10 and 30 µg/ml) were treated for 12 h. The cells were stained with 1 µM calcein-AM for 30 min at 37°C. The retention of calcein in live cells was used as a readout and the percentage of cell lysis (% of fluorescent cells among 10 000 counted cells) was calculated by FACSVerse (BD Biosciences) and FlowJo software (TreeStar, Ashland, OR, USA).

Purification of peripheral blood mononuclear cells (PBMCs)

PBMCs were purified from the 10 ml total blood of healthy donors who voluntarily participated in the study, which was conducted according to institutional review board (IRB) procedures approved by the committee of the Yonsei severance IRB board. All procedures were approved by the IRB (no. 4-2016-0600). The FcγRIII genotype of the blood was the Val/Phe heterozygote, as confirmed by sequencing of a 249 base-pair polymerase chain reaction (PCR) fragment using primers (sense; GTGGGTGTTCAAGGAGGAAG; anti-sense GTGGCACATGTCTCACCTTG). Briefly, 4 ml blood samples were centrifuged at 1600 g. The serum was removed and the cells were resuspended in 8 ml of PBS, followed by loading onto 4 ml of Ficoll (Histopaque-1077; Sigma, 10771) and centrifuged at 400 g for 35 min at 20°C to separate the white blood cells from the red blood cells. The white blood cell layer was collected into new tubes and washed three times (centrifuged at 300 g for 10 min) with RPMI media to completely remove the platelets. Purified PBMCs were counted and then incubated in RPMI media until use.

Measurement of antibody-mediated cell death

To measure the ADCC assay, 1×10^5 Ramos cells/well were loaded with 1 µM calcein-AM and incubated for 30 min at 37°C. Healthy viable cells were collected by evaluating calcein fluorescence. The cells were resuspended in 100 µl of media, different doses of antibody (0.1, 0.3, 1.3 and 10 µg/ml) were added and treated for 10 min. Next, 5×10^3 purified PBMCs (PBMC: Ramos = 1 : 20) were incubated at 37°C in a CO₂ incubator for 2 h. To determine the effect of the cell lysate on ADCC activity, the cell lysate homogenized in a 1 ml syringe was added during PBMC incubation. The percentage of lysate indicates the percentage of total Ramos cells used in the ADCC assay. The percentage of cells which lost fluorescence among 10 000 counted total cells was calculated with FACSVerse (BD Biosciences) and FlowJo software.

Single live cell $[Ca^{2+}]_c$ imaging

For Ca^{2+} imaging experiments, NaCl, KCl (P5405), $MgCl_2$ (M8266), glucose (G6152), HEPES (H3375), $CaCl_2$ (C1016), EGTA (E3889) and Fura-2 AM (F1201; Molecular Probes, Eugene, OR, USA) were used. Single live cell $[Ca^{2+}]_c$ imaging was performed by recording $[Ca^{2+}]_c$ with Fura-2 AM labelling at dual excitation wavelengths of 340/380 nm ratiometrically. HEK293T cells ($5-10 \times 10^4$) were plated on 18-mm ϕ cover glass (Paul Marienfeld GmbH & Co. KG, Lauda-Königshofen, Germany). After transfection, the cells were mixed with cell-permeable 2 μ M Fura-2 AM and incubated at 37°C, 5% CO_2 for 30 min, and trapped Fura-2 fluorescence was measured with a spectrofluorometer (Photon Technology International, Birmingham, NJ, USA). Cells were perfused with a solution composed of 150 mM NaCl, 5 mM KCl, 1 mM $MgCl_2$, 10 mM glucose, 10 mM HEPES (pH 7.4 adjusted with NaOH) and either 2 mM $CaCl_2$ or 5 mM EGTA (to chelate Ca^{2+} in the solution). The osmolality (osm) of all solutions was adjusted to 310 osm with the major salt. The Fura-2 ratio was recorded at dual-excitation wavelengths of 340/380 nm, and emission wavelengths above 510 nm were monitored. The cells were treated with 5 μ M thapsigargin (TG), which inhibits endoplasmic reticulum Ca^{2+} -ATPase. The cells were treated with 2 mM $CaCl_2$ and then each single whole cell boundary was drawn and intracellular Ca^{2+} concentrations ($[Ca^{2+}]_c$) were analysed.

Immunoprecipitation

HEK293T cells were seeded into six-well plates at 1×10^6 cells/well and incubated at 37°C, 5% CO_2 overnight. siRNA for siSTIM1 was transfected with RNAimax (Invitrogen) before transfection for over-expression. The plasmid was transfected with lipofectamine 2000 and expressed for 48 h. In samples treated with TG, 5 μ M TG was added and then the cells were harvested. Cells were lysed in lysis buffer (150 mM NaCl, 5 mM Na-EDTA, 10% glycerol, 20 mM Tris-HCl pH 8.0, 0.5% Triton X-100 and complete proteinase inhibitors) and the protein concentration was quantified by the Bradford Protein Assay. The lysates (~500 μ g of protein) in 400 μ l for each condition were mixed with anti-myc antibody (9E10; Santa Cruz Biotechnology for STIM1) and incubated overnight at 4°C. Antibody-bound complexes were precipitated using Protein A beads (Thermo Fisher Scientific) and washed three times with lysis buffer. The precipitates were eluted from the beads with $\times 2$ SDS sample buffer and separated on 4–12% pre-made gradient SDS-PAGE gels. Appropriate antibodies were used to detect the precipitated proteins and HRP-conjugated secondary antibody and ECL solution (Amersham Bioscience, Amersham, UK) were used for detection by chemiluminescence.

Immunocytochemistry

Ramos cells were prepared under appropriate conditions and fixed in 4% paraformaldehyde in PBS for 10 min at room temperature, followed by washing three times with PBS. The cells were treated with blocking solution (5% horse serum, 1% BSA, 0.1% gelatine, 0.001% sodium azide in PBS pH 7.4) at room temperature for 30 min. The first immunostaining was performed in blocking solution with rituximab and obinutuzumab, followed by secondary anti-Fc specific human IgG conjugated with FITC. Next, 0.1% Triton X-100 in PBS was used to permeabilize the cells, and caveolin was stained with an anti-caveolin1 antibody (cat no. E18-6386; EnoGene, New York, NY, USA) followed by visualization with anti-rabbit IgG-specific secondary antibody conjugated to Alexa 350 (blue). To stain STIM1, 0.5% Triton X-100 in PBS was used to permeabilize and dissolve the Triton-soluble membrane. Next, anti-STIM1 and secondary anti-mouse IgG conjugated with Alexa Fluor-rhodamine was used. The coverslips were rinsed and the cells were mounted with fluorescent mounting medium (S3023; Dako, Glostrup, Denmark) and visualized by confocal microscopy (LSM 780 controlled with Zen software; Carl Zeiss, Jena, Germany).

Quantification of binding affinity test

To compare the binding affinities of the antibodies for the scramble- and siSTIM1-transfected Ramos cells, flow cytometry [fluorescence-activated cell sorter (FACS); BD Biosciences] was used. Scramble- or siSTIM1-transfected Ramos cells (5×10^5) were incubated with rituximab and obinutuzumab at 10 μ g/ml for 15 min on ice followed by incubation with anti-human Ig Fc-specific FITC-conjugated secondary antibody (109-095-008; Jackson Laboratories) for 30 min at 4°C. The cells were washed twice with culture medium, and then the FITC fluorescence under each condition was analysed by fluorescence-activated cell sorting. An anti-human Ig Fc-specific FITC-conjugated antibody-treated sample was used as a negative control. The binding level was measured as the mean fluorescence intensity of each sample.

Quantification of raft-localized CD20 through Triton solubility test

Scramble- or siSTIM1-transfected 5×10^6 Ramos cells were incubated at 37°C for 30 min in complete culture medium either alone or supplemented with 10 μ g/ml rituximab or obinutuzumab, and the cells were treated with secondary FITC-conjugated anti-human Fc-specific IgG antibody and divided into two samples. In each sample, one part was treated with PBS while the other part was

treated with 0.5% Triton in PBS for 15 min and washed twice with PBS. Antibody fluorescence under each condition was measured by fluorescence-activated cell sorting. The mean fluorescence intensity (MFI) of Triton-treated cells/MFI of PBS-treated cells indicated the relative Triton solubility of the antibody.

Statistical analysis

The results of multiple experiments are presented as mean ± standard error of the mean (s.e.m.), and statistical analysis was performed using analysis of variance (ANOVA) or Student's *t*-test, as appropriate, via GraphPad Prism

software (version 5.0; GraphPad, Inc., La Jolla, CA, USA). *P* < 0.05 was considered statistically significant.

Results

Store-operated Ca²⁺ influx activity of CD20 depends on Orai1 and STIM1

We investigated the Ca²⁺ influx channel function of CD20 as an SOC to determine whether the function of CD20 is regulated by Orai1 and STIM1, the core proteins affecting store-operated Ca²⁺ influx (Fig. 1a,b).

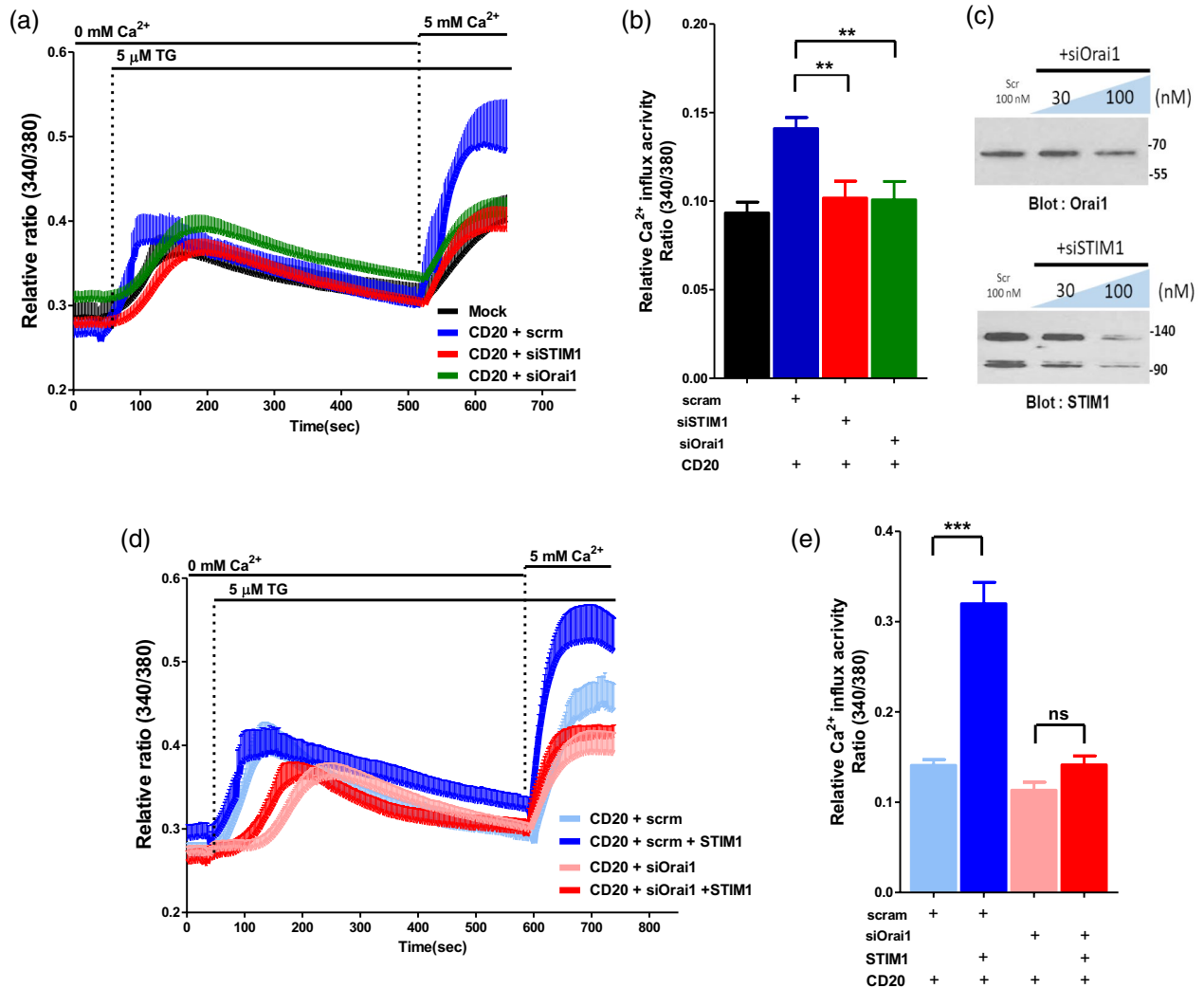


Fig. 1. CD20 store-operated Ca²⁺ influx activity is regulated by Orai1 and stromal interaction molecule (STIM1). (a) Trace of Ca²⁺ changes by CD20 dependent on Orai1 and STIM1 in human kidney embryo (HEK) cells. Scramble short interfering RNA (siRNA), siRNA specific for Orai1 and siRNA specific for STIM1 were pretransfected into HEK cells, and then CD20 was over-expressed. After loading of Fura-2 AM, live cell fluorescence changes were recorded. (b) Summary of Ca²⁺ influx activity (Δ ratio 350 : 380). At least 30 cells under each condition were used for calculation. ***P* ≤ 0.01. (c) Western blotting for evaluation of the siRNA of Orai1 and STIM1 in HEK cells. (d) STIM1 co-expression increased the Ca²⁺ influx of CD20, but this increase was abolished by siOrai1. After scramble-siRNA or siRNA for Orai1 were treated, HEK cells over-expressed CD20 alone or CD20 plus STIM1, and the same experiments described in (a) were performed. (e) Summary of experiments in (c). ***P* ≤ 0.01. Immunoprecipitation assay using myc antibody (for STIM1) and Flag antibody (for CD20 and Orai1).

Functional analysis showed that CD20 over-expression increased Ca^{2+} influx. This increased TG-induced Ca^{2+} influx activity was abolished in siOrai1- and siSTIM1-treated cells. The knock-down effects were validated with Western blotting analysis for each siOrai1 and siSTIM1 (Fig. 1c). Additionally, TG-stimulated STIM1 co-expression, which enhanced Ca^{2+} influx through CD20, disappeared under Orai1 knock-down conditions (Fig. 1d,e). This functional analysis revealed that CD20 acts as an SOC by interacting with Orai1 and that STIM1 regulation of the SOC function of CD20 depends on Orai1 expression.

Enhanced protein interaction of CD20 and STIM1 under store-depleted condition of HEK cells

To evaluate the interaction between CD20, STIM1 and Orai1, we performed an immunoprecipitation assay under Orai1 over-expression and knock-down conditions (Fig. 2a-c). TG (5 μ M) enhanced the CD20 interaction with STIM1, and the constitutively active form of STIM1 strongly interacted with CD20 (Fig. 2a). Furthermore, this interaction was not observed under siOrai1-treated conditions (Fig. 2b). CD20 and STIM1 co-localization was strengthened by 5 μ M TG using immunocytochemistry analysis (Fig. 2c) and CD20 and STIM1 expression (Supporting information, Fig. S1),

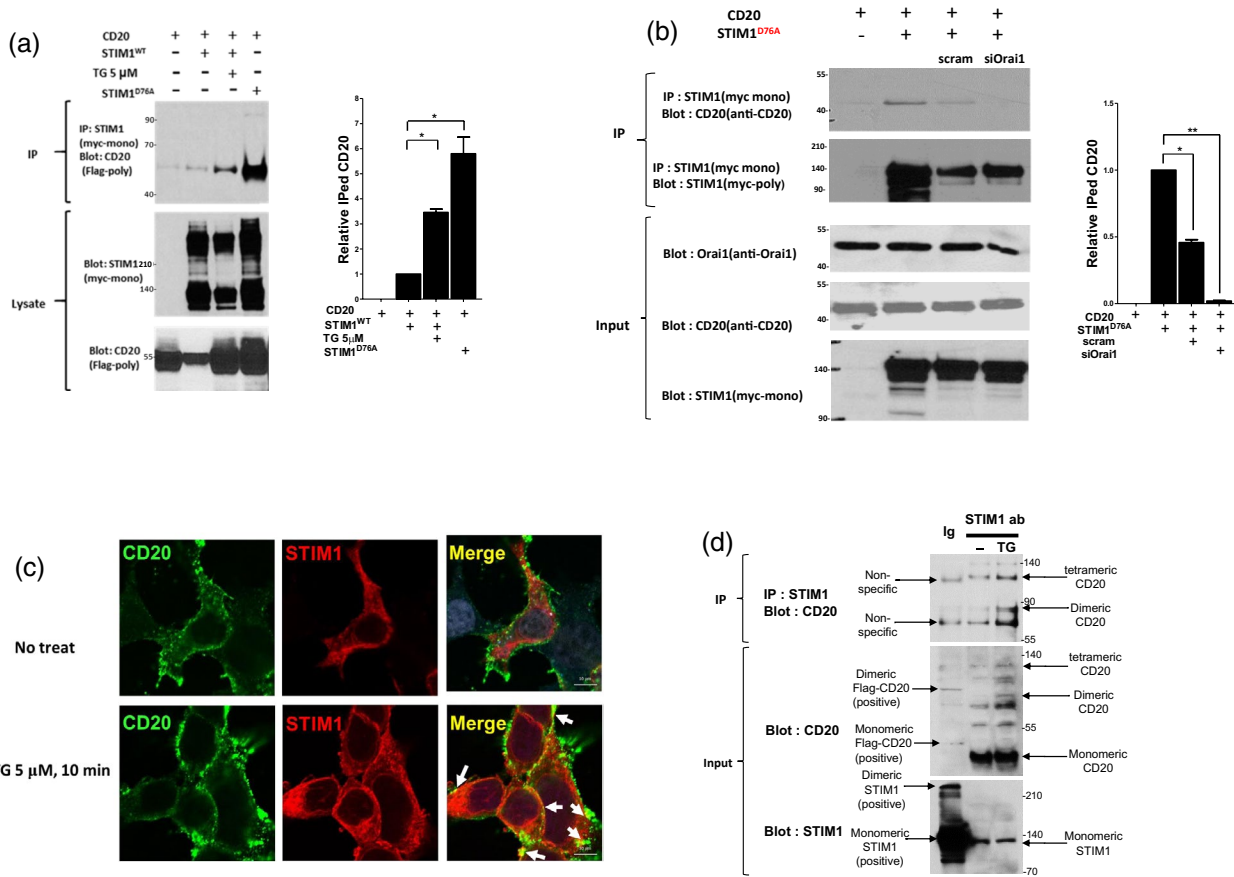


Fig. 2. Enhanced protein interaction of CD20 and stromal interaction molecule (STIM1) under store-depleted conditions of human kidney embryo (HEK) cells with overexpression of Flag-CD20 and myc-STIM1 (a). Thapsigargin (TG) (5 μ M, 10 min) and STIM1^{D76A} (constitutively active form) were used to show the enhanced protein interaction under the store depletion condition. Expression levels of STIM1 and CD20 were evaluated by Western blot analysis using myc and Flag antibodies to detect STIM1 and CD20, respectively. (b) Knock-down of Orai1 decreased the CD20 interaction with STIM1^{D76A}. (c) CD20 and STIM1 localization under normal conditions (upper) and store depletion conditions (5 μ M TG for 10 min) (bottom) in HEK cells. CD20 and STIM1 were labelled with anti-Flag [secondary antibody conjugated with fluorescein isothiocyanate (FITC) (green)] and anti-STIM1 [secondary antibody conjugated with rhodamine (red)]. Merged image showing their co-localization (yellow) under store depletion conditions. White arrow indicates co-localized CD20 with STIM1. Bar indicates 10 μ m. (d) Endogenous protein interaction of CD20 and STIM1 was observed in immunoprecipitation assay using Ramos cell lysate. Resting and store-depleted condition lysate was immunoprecipitated with monoclonal anti-STIM1 antibody and precipitated CD20 was identified with goat anti-CD20 antibody. Mouse immunoglobulin (Ig)G was used as control for immunoprecipitation analysis. In inputs, each over-expressed CD20 and STIM1 was used as a positive control in Western blotting. Each protein is indicated as shown.

and their interaction was confirmed in Ramos cells (Fig. 2d). These data indicate that CD20 interacts with STIM1, which largely depends upon Orai1 expression.

Extracellular Ca^{2+} concentration is critical for homotypical adhesion, but not for obinutuzumab binding-induced cell death

Few studies have evaluated the effect of CD20 calcium influx on the binding-induced cell death caused by obinutuzumab. We presumed that the ion pore activity of CD20 affects the direct cell death mechanism of obinutuzumab. Dose-dependent cell death caused by obinutuzumab binding was confirmed in the presence and absence of Ca^{2+} . Unexpectedly, cell death induced by obinutuzumab binding occurred with (1.5 mM CaCl_2 ; RPMI media) and without Ca^{2+} (approximately 500 nM Ca^{2+} ; 1 mM EGTA RPMI media), and Ca^{2+} low conditions were associated with higher cell death rates at each dose (Fig. 3a). To compare cell death at lower Ca^{2+} concentrations (Fig. 3b), we compared this rate in a solution of 2 mM Ca^{2+} and 67 nM Ca^{2+} (2 mM Ca^{2+} , 2 mM EGTA). Interestingly, extracellular EGTA conditions showed enhanced cell death upon obinutuzumab binding. In contrast, homotypical adhesion during cell death by obinutuzumab binding was observed only in the presence of calcium (Fig. 3c). CD20 capping by rituximab, the location of which was indicated by caveolin

antibody, also disappeared under low Ca^{2+} conditions (Fig. 3d). These results indicate that the Ca^{2+} pore function of CD20 does not affect the cell death process induced by obinutuzumab binding. Additionally, homotypical adhesion appears to be Ca^{2+} -dependent, which is not the cause of cell death.

Rituximab and obinutuzumab binding induced no fluorescence changes of GCaMP-CD20

Next, to answer the obvious question of whether rituximab and obinutuzumab binding cause Ca^{2+} influx through CD20, we monitored GCaMP-CD20 fluorescence changes after treatment of each antibody. (Fig. 4). First, we checked the appropriate fluorescence changes upon TG-stimulated Ca^{2+} influx near GCaMP-CD20 (Fig. 4a. Supporting information, Movie S1). No fluorescence changes at TG treatment, but an apparent fluorescence increase at 5 mM extracellular Ca^{2+} , shows that GCaMP-CD20 fluorescence indicates Ca^{2+} changes only near CD20. The summary of three experiments are graphed in Fig. 4b. Next, each antibody-induced fluorescence change was recorded, as summarized in Fig. 4c–f. Fluorescence was started to record Ca^{2+} free solution and 5 mM Ca^{2+} was treated to observe spontaneous Ca^{2+} influx, then each antibody was treated to observe the antibody binding-induced fluorescence changes. Then, 100 μM adenosine triphosphate (ATP) was treated to observe that the cell fluo-

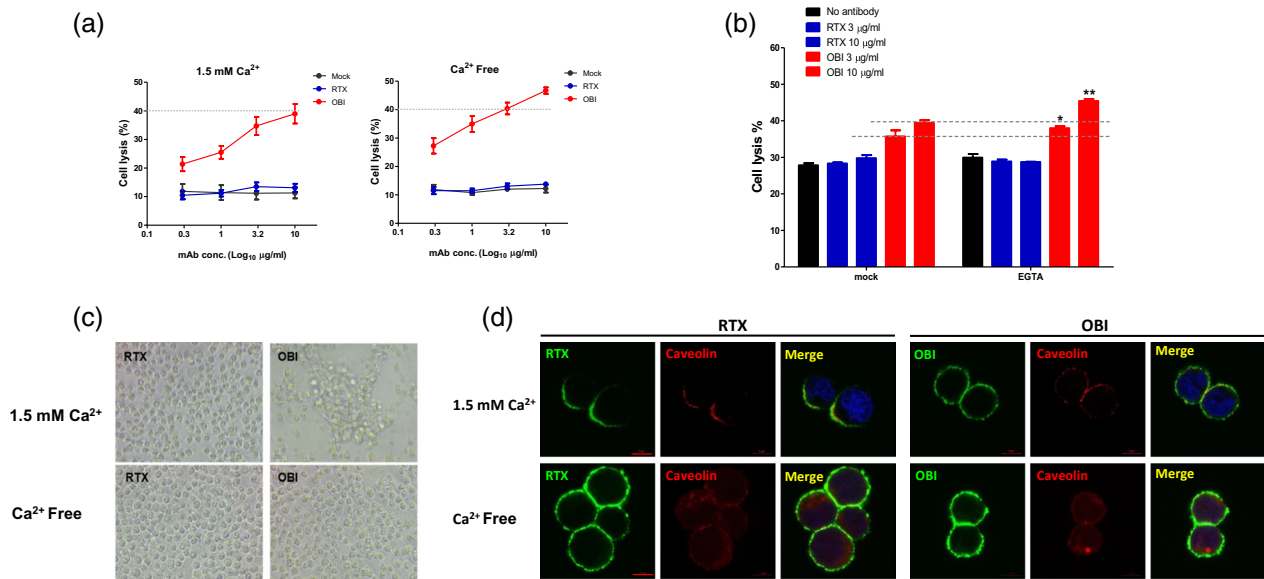


Fig. 3. Extracellular Ca^{2+} concentration is critical for homotypical adhesion but not for obinutuzumab binding-induced cell death (a) Obinutuzumab binding-induced cell death was analysed in RPMI medium (1.5 mM Ca^{2+}) and Ca^{2+} low conditions [1 mM ethylene glycol tetraacetic acid (EGTA) containing RPMI, approximately 500 nM Ca^{2+}]; 0.3, 1, 3 and 10 $\mu\text{g}/\text{ml}$ of each antibody was treated, and the cell death rate was measured after 24 h. (b) Binding-induced direct cell death by 3 and 10 $\mu\text{g}/\text{ml}$ of rituximab and obinutuzumab under intra- and extracellular Ca^{2+} -chelating conditions and 2 mM Ca^{2+} or 67 nM low Ca^{2+} regular solution (2 mM EGTA in 2 mM Ca^{2+}). (c) Homotypical adhesion by antibodies in 2 mM Ca^{2+} or 500 nM Ca^{2+} condition visualized by light microscopy. (d) Rituximab and obinutuzumab-induced CD20 localization with or without external Ca^{2+} . Each condition was visualized by rituximab and obinutuzumab immunostaining. Raft region is indicated by caveolin antibody. Bar, 5 μm .

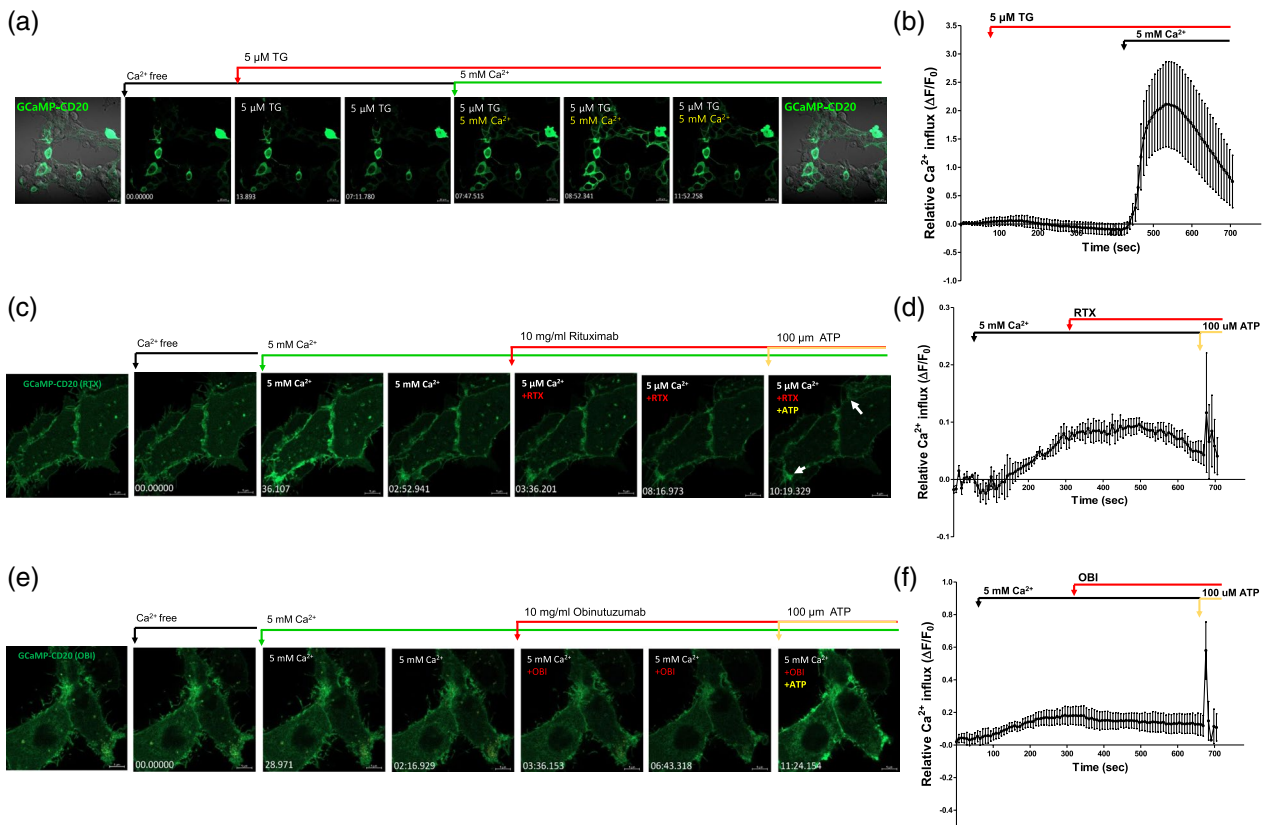


Fig. 4. Rituximab and obinutuzumab do not cause Ca^{2+} influx near CD20. (a) GCaMP-CD20 fluorescence changes upon 5 μM thapsigargin (TG) and then 5 mM Ca^{2+} was added to show the store-operated characteristics of CD20. TG treatment did not cause any fluorescence changes, but 5 mM Ca^{2+} addition evoked dramatic fluorescence changes in very weak fluorescent cells. Lower left: recording time (minute : second), Bar, 20 μm . (b) Summary of three independent experiments of more than 30 cells fluorescence changes. GCaMP-CD20 fluorescence changes upon rituximab (c,d) and obinutuzumab (e,f) treatment; 5 mM Ca^{2+} was treated to show the spontaneous Ca^{2+} increase then 10 mg/ml rituximab (c) and obinutuzumab (e) was treated. Finally, 100 μM adenosine triphosphate (ATP) was treated to check the valid fluorescence response. (d,f) Summary of three independent experiments of more than 10 cells fluorescence changes. Lower left: recording time (minute : second), Bar, 5 μm .

rescence responded appropriately. As shown in Fig. 4c,e (Supporting information, Movies S2 and S3), neither rituximab nor obinutuzumab induced fluorescence change of GCaMP-CD20. These data imply that rituximab and obinutuzumab binding did not cause any Ca^{2+} influx through or nearby CD20.

Binding affinity of obinutuzumab was reduced by STIM1 knock-down

Obinutuzumab is known to have an inter-tetrameric binding mode by binding to open-form CD20 [25]. It is also known to bind CD20 present in the non-raft membrane part of soluble Triton [9,25]. Because STIM1 binds to CD20, we hypothesized that binding of STIM1 would affect the binding of rituximab or obinutuzumab to CD20.

To determine the localization of STIM1 in rituximab- or obinutuzumab-treated Ramos cells, we performed immunostaining with a cell membrane permeabilization step induced by 0.5% Triton solution to dissolve the non-raft

region (Fig. 5a,b). Ramos cells fixed before rituximab or obinutuzumab binding were used to indicate the normal localization of CD20 and STIM1. When cells were fixed before rituximab or obinutuzumab treatment and 0.5% Triton permeabilization (control), each antibody was easily observed throughout the plasma membrane, with STIM1 also clearly observed near the membrane region (Fig. 5a, control in first and third row), while STIM1 staining in rituximab-treated cells was weaker. As shown in Fig. 5b, line scan images across the cells (crossing arrow in merged images in Fig. 5a) revealed the amount and localization of the antibody and STIM1. When the cells were pretreated with rituximab before fixation, capping of CD20 was observed and STIM1 localization was similar to the rituximab distribution. Interestingly, when the cells were pretreated with obinutuzumab before fixation followed by 0.5% Triton permeabilization, frequent loss of obinutuzumab staining was observed and the STIM1 signal almost disappeared (pretreated OBI, last row). This suggests that

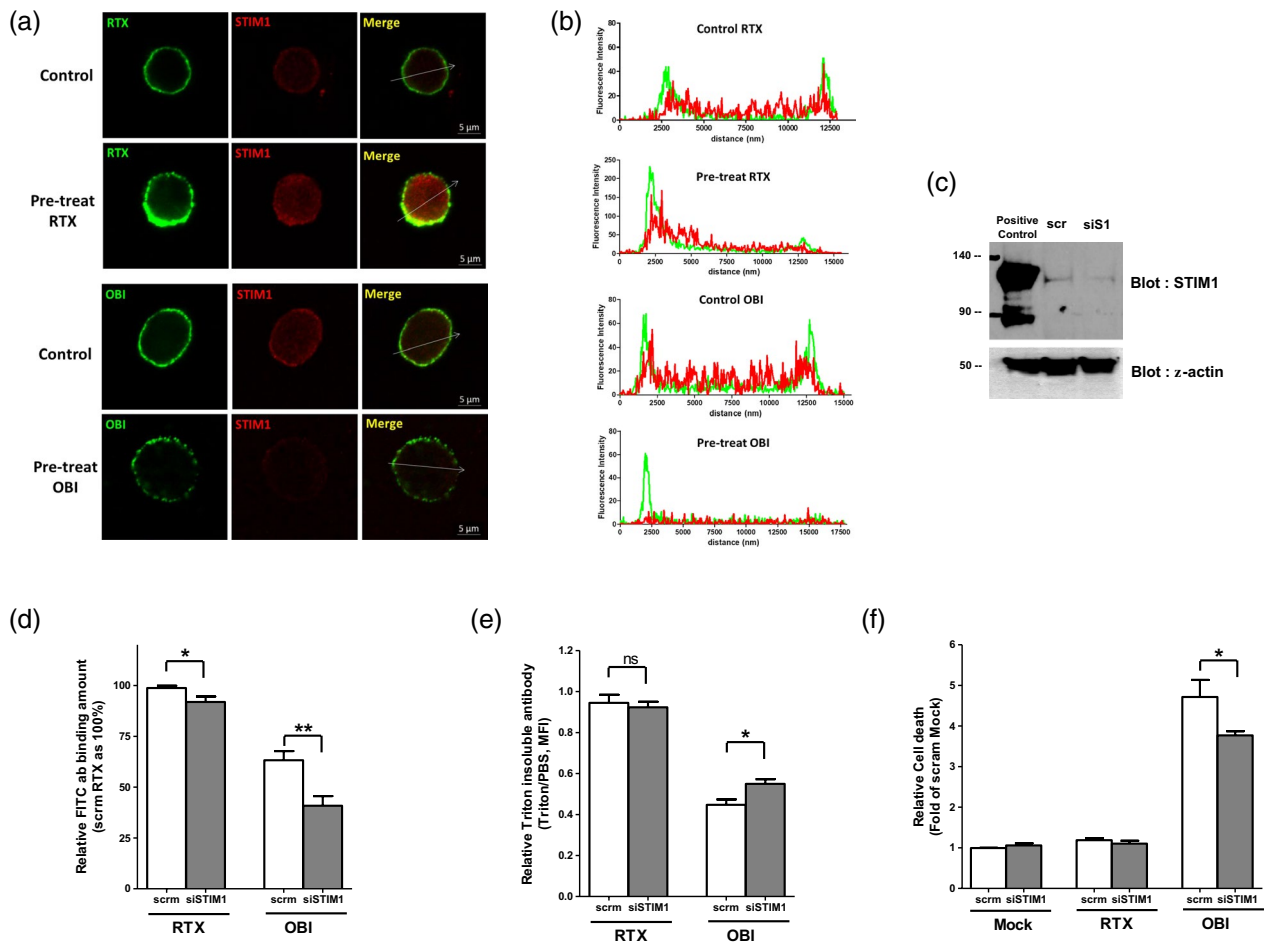


Fig. 5. Obinutuzumab-bound CD20 is complexed with stromal interaction molecule (STIM1). (a) Immunostaining with cell membrane permeabilization step using 0.5% Triton solution to dissolve the non-raft region to discriminate the localization of CD20 in raft or non-raft region after each antibody binding. Ramos cells were fixed before rituximab or obinutuzumab treatment was used for control. Bar: 5 μ m. Cells pretreated with each antibody (green) then fixed are indicated as pretreated. The cells were then permeabilized for STIM1 staining (red). (b) Line scan images across the cells (crossing arrow in merged images on the right in most images) indicates the distribution of CD20 (green) and STIM1 (red) in across cells. (c) Protein expression of STIM1 was significantly reduced by short interfering RNA (siRNA) in Ramos cells. (d) To test the binding properties of CD20 upon STIM1 knock-down, Ramos cells transfected with scramble or siS1STIM1 were treated with rituximab or obinutuzumab, and then binding was quantified using fluorescein isothiocyanate (FITC)-conjugated secondary antibodies. (e) To test the raft localization of CD20 upon STIM1 binding, their Triton-insoluble levels were quantified with FITC-conjugated secondary antibodies after 0.5% Triton or phosphate-buffered saline (PBS) treatment. (f) Binding-induced cell death was observed in STIM1 knock-down Ramos cells by siRNA for STIM1. Antibody (3 μ g/ml) was treated for 24 h. * $P \leq 0.05$; ** $P \leq 0.01$.

STIM1-captured CD20 bound to obinutuzumab is localized in the Triton-soluble membrane.

If binding of obinutuzumab to Triton-soluble CD20 in Ramos cells is associated with STIM1, the degree of obinutuzumab binding may be affected and STIM1 expression is altered. To confirm this, we evaluated the binding capacity of obinutuzumab by using Ramos cells expressing STIM1 siRNA (Fig. 5d); knock-down efficiency was determined by Western blot analysis in Fig. 5c. When STIM1 expression was knocked down, the amount of bound rituximab somewhat decreased, while binding of obinutuzumab was decreased more significantly (Fig. 5d). Next, the Triton

solubility of each antibody was confirmed when STIM1 expression was decreased (Fig. 5e). When STIM1 expression was decreased, Triton-resistant rituximab binding was not affected while Triton-resistant obinutuzumab binding was increased. This suggests that the STIM1 bound to CD20 was soluble in Triton, and that the configuration of this binding is favourable for obinutuzumab binding. Finally, to confirm whether or not the expression level of STIM1 affects cell death by obinutuzumab binding, direct cell death by obinutuzumab was observed under STIM1 knock-down conditions (Fig. 5f). We found that obinutuzumab binding-induced cell death was significantly decreased under STIM1

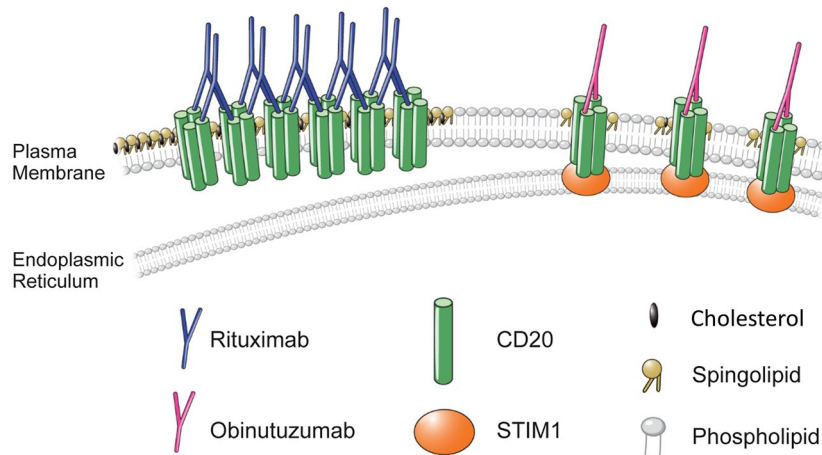


Fig. 6. A model for the preferred binding of obinutuzumab on stromal interaction molecule (STIM1)-bound CD20, rituximab bound to CD20 and aggravated CD20 in the cholesterol-rich raft region, which is insoluble by 0.5% Triton. Meanwhile, obinutuzumab binds to CD20, which is located by STIM1 binding in the non-raft region. Upon binding of each antibody, no Ca^{2+} influx occurs though only CD20.

siRNA-treated conditions. This result was also observed when STIM1 expression was decreased by Cas-9-mediated gene knock-down (Supporting information, Fig. S2). Thus, CD20 may interact with STIM1, which has a high affinity for obinutuzumab and appears to localize in the non-raft region, which may contribute to the efficacy of direct binding-mediated cell death via obinutuzumab.

Discussion

In this study, we found that obinutuzumab preferred to bind to STIM1-localized CD20, where the Triton-soluble region of membrane (Fig. 6) CD20 is apparently a co-working component for store-operated Ca^{2+} influx pore-dependent on Orai1 expression. However, we found two proofs that Ca^{2+} influx of CD20 is not involved in the obinutuzumab binding-induced cell death. First, obinutuzumab binding-induced cell death occurred in extracellular Ca^{2+} free conditions. Secondly, obinutuzumab binding could not induce Ca^{2+} influx or Ca^{2+} signal in fluorescence change monitoring using GCaMP-CD20.

In Fura2-AM, using Ca^{2+} signal measurement in CD20-expressing cells, the Ca^{2+} can be influxed from outside, although CD20 and Ca^{2+} also can be evoked from the intracellular Ca^{2+} reservoir, which hinders tracking the exact source of Ca^{2+} . Conversely, GCaMP-CD20 can show Ca^{2+} concentration changes only near CD20 (Fig. 4c–f), which confirmed the exact source of Ca^{2+} after obinutuzumab binding. Using this method, we confirm that obinutuzumab does not cause Ca^{2+} influx through or near CD20.

Type I and Type II antibodies have very different characteristics [9,35]. Type I requires an extremely long time to induce apoptosis, whereas Type II induces relatively fast cell death by epitope binding alone. Previously, Shan *et al.* have

reported that malignant human B cells undergo apoptosis by ligation of CD20 with monoclonal antibodies [36]. In this study they used 1F5 monoclonal antibody, which is a Type I antibody similar to rituximab [35]. They also found that apoptosis by 1F5 was reduced by BAPTA-AM and EGTA extracellular treatment [36]. This is in contrast to our results, which showed the same or a slightly higher apoptosis rate under EGTA condition. This difference suggests that intracellular signalling mechanisms by Type I and the cell death-related signalling events by binding Type II may be different. In the follow-up study, we will further investigate whether the phenomenon more effective in the absence of extracellular calcium, such as endocytosis, is related to the cell-death mechanism by obinutuzumab binding.

The epitope regions of rituximab and obinutuzumab contain the same extracellular large loop of CD20 according to epitope-finding analysis using amino acid scanning [25]. However, the configurations of CD20 binding to antibodies, including the binding angles of each antibody, differ from the results of structural analysis [8]. Therefore, the configuration of CD20 probably determines the binding mode of antibodies and contributes to the potency of B cell depletion. The binding affinity and DCD of obinutuzumab were attenuated by the knock-down of STIM1 expression using siRNA for STIM1 (Fig. 4d,f). In addition, non-raft-localized CD20 was decreased by siSTIM1-treated Ramos cells (Fig. 4e). These data imply that STIM1 binding to CD20 leads to a more favourable configuration of CD20 that is optimized for obinutuzumab binding. In addition, these results support the idea that the CD20 exists in two distinct configurations (lipid raft form and non-lipid raft form), whose respective functions differ. Rituximab-bound CD20 capped at the raft region is involved in B cell receptor activation and FcRII-involved

internalization [20,37]. In contrast, obinutuzumab-bound CD20 is localized in the non-raft region, where the membrane shows high fluidity and the potential for endocytosis. These characteristics of the membrane region may be related to lysosomal rupture by obinutuzumab. In-depth studies of endocytosis caused by obinutuzumab binding to the STIM1 anchoring CD20 region may reveal how lysosomal rupture occurs after obinutuzumab binding.

Homotypical adhesion (HA), a typical phenomenon caused by obinutuzumab, is known as a main cause of DCD. The actin-immobilizing drugs latrunculin and actinomycin inhibited HA and cell death caused by obinutuzumab binding, indicating that HA causes cell death [9,18]. However, our study revealed that HA is a secondary event occurring after obinutuzumab binding-induced cell death because HA is a Ca^{2+} -dependent phenomenon, while external Ca^{2+} did not affect cell death induced by obinutuzumab binding. The previous finding, that cell death caused by binding is inhibited via actin immobilizing agents, is correct, because another actin-mobilizing event such as endocytosis can be related to obinutuzumab-induced cell death.

The basic molecular mechanism including the interactions between CD20 and its antibody are not well understood, while many studies have examined the clinical efficacy of CD20 antibodies. In particular, although previous studies have shown that CD20 over-expressing cells exhibit store-operated Ca^{2+} entry activity [15,16], the molecular mechanism of the channel activity of CD20 and its effect on antibody function remain unclear. In our study, we found that the store-operated mode of Ca^{2+} influx of CD20 is mediated by Orai1 and STIM1. Enhanced Ca^{2+} influx by STIM1 is dependent upon the presence of Orai1 (Fig 2). These data suggest that CD20 participates in forming the SOC pore with Orai1, which is regulated by store depletion and STIM1. However, the Ca^{2+} free condition showed higher rates of cell death upon obinutuzumab binding, and thus the SOC of CD20 is not involved in obinutuzumab binding-induced cell death.

In conclusion, we suggest that obinutuzumab is recognized as an improved bio-better because of the characteristics of DCD as well as the ADCC of obinutuzumab, and that even the ability of ADCC can be influenced by DCD. In this study, we propose that one of the mechanisms underlying this important DCD ability of obinutuzumab is the more obinutuzumab-friendly configuration of the STIM1 binding sites of CD20, which increases DCD.

Acknowledgements

This work was supported by grants from the National Research Foundation of Korea, Project no. NFR-2018R1A2B4010319, and a faculty research grant from the Yonsei University College of Medicine (6-2018-0070) to J.

Y. K. The authors thank MID (Medical Illustration and Design), a part of the Medical Research Support Services of Yonsei University College of Medicine, for all artistic support related to this work.

Disclosures

No potential conflict of interest reported by the authors.

References

- 1 Rogers LM, Veeramani S, Weiner GJ. Complement in monoclonal antibody therapy of cancer. *Immunol Res* 2014; **59**:203–10.
- 2 Romero D. Alliance to iLLUMINATE the chemo-free sign. *Nat Rev Clin Oncol* 2019; **16**:65.
- 3 Mossner E, Brunker P, Moser S *et al.* Increasing the efficacy of CD20 antibody therapy through the engineering of a new type II anti-CD20 antibody with enhanced direct and immune effector cell-mediated B-cell cytotoxicity. *Blood* 2010; **115**:4393–402.
- 4 Herter S, Herting F, Mundigl O *et al.* Preclinical activity of the type II CD20 antibody GA101 (obinutuzumab) compared with rituximab and ofatumumab in vitro and in xenograft models. *Mol Cancer Ther* 2013; **12**:2031–42.
- 5 Salles GA, Morschhauser F, Solal-Celigny P *et al.* Obinutuzumab (GA101) in patients with relapsed/refractory indolent non-Hodgkin lymphoma: results from the phase II GAUGUIN study. *J Clin Oncol* 2013; **31**:2920–6.
- 6 Cartron G, de Guibert S, Dillhuydy MS *et al.* Obinutuzumab (GA101) in relapsed/refractory chronic lymphocytic leukemia: final data from the phase 1/2 GAUGUIN study. *Blood* 2014; **124**:2196–202.
- 7 Marcus R, Davies A, Ando K *et al.* Obinutuzumab for the First-Line Treatment of Follicular Lymphoma. *N Eng J Med* 2017; **377**:1331–44.
- 8 Jak M, van Bochove GG, Reits EA *et al.* CD40 stimulation sensitizes CLL cells to lysosomal cell death induction by type II anti-CD20 mAb GA101. *Blood* 2011; **118**:5178–88.
- 9 Alduaij W, Ivanov A, Honeychurch J *et al.* Novel type II anti-CD20 monoclonal antibody (GA101) evokes homotypical adhesion and actin-dependent, lysosome-mediated cell death in B-cell malignancies. *Blood* 2011; **117**:4519–29.
- 10 Tedder TF, Klejman G, Disteche CM, Adler DA, Schlossman SF, Saito H. Cloning of a complementary DNA encoding a new mouse B lymphocyte differentiation antigen, homologous to the human B1 (CD20) antigen, and localization of the gene to chromosome 19. *J Immunol* 1988;**141**:4388–94.
- 11 Walport M, Murphy K, Janeway C, Travers PJ. *Janeway's Immunobiology*, 7th edn. Abingdon, UK: Taylor & Francis; 2008.
- 12 Bubien JK, Zhou LJ, Bell PD, Frizzell RA, Tedder TF. Transfection of the CD20 cell surface molecule into ectopic cell types generates a Ca^{2+} conductance found constitutively in B lymphocytes. *J Cell Biol* 1993; **121**:1121–32.
- 13 Polyak MJ, Tailor SH, Deans JP. Identification of a cytoplasmic region of CD20 required for its redistribution to a detergent-insoluble membrane compartment. *J Immunol* 1998;**161**:3242–8.

- 14 Li H, Ayer LM, Polyak MJ *et al.* The CD20 calcium channel is localized to microvilli and constitutively associated with membrane rafts: antibody binding increases the affinity of the association through an epitope-dependent cross-linking-independent mechanism. *J Biol Chem* 2004; **279**:19893–901.
- 15 Li H, Ayer LM, Lytton J, Deans JP. Store-operated cation entry mediated by CD20 in membrane rafts. *J Biol Chem* 2003; **278**:42427–34.
- 16 Vacher P, Vacher AM, Pineau R *et al.* Localized store-operated calcium influx represses CD95-dependent apoptotic effects of rituximab in non-Hodgkin B lymphomas. *J Immunol* 2015; **195**:2207–15.
- 17 Walshe CA, Beers SA, French RR *et al.* Induction of cytosolic calcium flux by CD20 is dependent upon B Cell antigen receptor signaling. *J Biol Chem* 2008; **283**:16971–84.
- 18 Janas E, Priest R, Wilde JI, White JH, Malhotra R. Rituxan (anti-CD20 antibody)-induced translocation of CD20 into lipid rafts is crucial for calcium influx and apoptosis. *Clin Exp Immunol* 2005; **139**:439–46.
- 19 Daniels I, Turzanski J, Haynes AP. A requirement for calcium in the caspase-independent killing of Burkitt lymphoma cell lines by Rituximab. *Br J Haematol* 2008; **142**:394–403.
- 20 Polyak MJ, Li H, Shariat N, Deans JP. CD20 homo-oligomers physically associate with the B cell antigen receptor. Dissociation upon receptor engagement and recruitment of phosphoproteins and calmodulin-binding proteins. *J Biol Chem* 2008; **283**:18545–52.
- 21 Smith MR. Rituximab (monoclonal anti-CD20 antibody): mechanisms of action and resistance. *Oncogene* 2003; **22**:7359–68.
- 22 Reff ME, Carner K, Chambers KS *et al.* Depletion of B cells *in vivo* by a chimeric mouse human monoclonal antibody to CD20. *Blood* 1994; **83**:435–45.
- 23 Glennie MJ, French RR, Cragg MS, Taylor RP. Mechanisms of killing by anti-CD20 monoclonal antibodies. *Mol Immunol* 2007; **44**:3823–37.
- 24 Kern DJ, James BR, Blackwell S, Gassner C, Klein C, Weiner GJ. GA101 induces NK-cell activation and antibody-dependent cellular cytotoxicity more effectively than rituximab when complement is present. *Leuk Lymph* 2013; **54**:2500–5.
- 25 Niederfellner G, Lammens A, Mundigl O *et al.* Epitope characterization and crystal structure of GA101 provide insights into the molecular basis for type I/II distinction of CD20 antibodies. *Blood* 2011; **118**:358–67.
- 26 Klein C, Lammens A, Schafer W *et al.* Epitope interactions of monoclonal antibodies targeting CD20 and their relationship to functional properties. *mAbs* 2013; **5**:22–33.
- 27 Chan HT, Hughes D, French RR *et al.* CD20-induced lymphoma cell death is independent of both caspases and its redistribution into triton X-100 insoluble membrane rafts. *Can Res* 2003; **63**:5480–9.
- 28 Roos J, DiGregorio PJ, Yeromin AV *et al.* STIM1, an essential and conserved component of store-operated Ca²⁺ channel function. *J Cell Biol* 2005; **169**:435–45.
- 29 Liou J, Kim ML, Heo WD *et al.* STIM is a Ca²⁺ sensor essential for Ca²⁺-store-depletion-triggered Ca²⁺ influx. *Curr Biol* 2005; **15**:1235–41.
- 30 Zhou Y, Srinivasan P, Razavi S *et al.* Initial activation of STIM1, the regulator of store-operated calcium entry. *Nat Struct Mol Biol* 2013; **20**:973–81.
- 31 Saheki Y, De Camilli P. Endoplasmic reticulum–plasma membrane contact sites. *Annu Rev Biochem* 2017; **86**:659–84.
- 32 Maleth J, Choi S, Muallem S, Ahuja M. Translocation between PI(4,5)P₂-poor and PI(4,5)P₂-rich microdomains during store depletion determines STIM1 conformation and Orai1 gating. *Nat Commun* 2014; **5**:5843.
- 33 Pani B, Ong HL, Liu X, Rauser K, Ambudkar IS, Singh BB. Lipid rafts determine clustering of STIM1 in endoplasmic reticulum–plasma membrane junctions and regulation of store-operated Ca²⁺ entry (SOCE). *J Biol Chem* 2008; **283**:17333–40.
- 34 Latour S, Zanese M, Le Morvan V *et al.* Role of calcium signaling in GA101-induced cell death in malignant human B cells. *Cancers (Basel)* 2019; **11**: pii:E291.
- 35 Beers SA, Chan CH, French RR, Cragg MS, Glennie MJ. CD20 as a target for therapeutic type I and II monoclonal antibodies. *Semin Hematol* 2010; **47**:107–14.
- 36 Shan D, Ledbetter JA, Press OW. Apoptosis of malignant human B cells by ligation of CD20 with monoclonal antibodies. *Blood* 1998; **91**:1644–52.
- 37 Vaughan AT, Chan CH, Klein C, Glennie MJ, Beers SA, Cragg MS. Activatory and inhibitory Fcγ receptors augment rituximab-mediated internalization of CD20 independent of signaling via the cytoplasmic domain. *J Biol Chem* 2015; **290**:5424–37.

Supporting Information

Additional supporting information may be found in the online version of this article at the publisher's web site:

Fig. S1. Endogenous protein expression and mRNA expression of CD20, STIM1, and Orai1 in Ramos cells. (a–c) Protein expression of Orai1 (a), CD20 (b), and STIM1 (c) in Ramos cells under mock and TG-treated conditions. Anti-Orai1 antibody, anti-CD20 antibody, and anti-STIM1 antibody were used to detect each protein. (d), Relative mRNA expression of CD20, STIM1, STIM2, Orai1, Orai2, and Orai3 in Ramos and HEK cells

Fig. S2. Cell death rate was reduced after STIM1 knock-down by Cas9-mediated gene editing. (a) Genome structure of STIM1 and location of sgRNAs of target1 and target2. (b) Knockdown expression of STIM1 in target1 and target2 sgRNA-mediated Cas9 gene editing. (c) Cell death by obinutuzumab binding in target1 (STIM1 cas9-1) and target2 (STIM1 cas9-2) sgRNA-treated STIM1 knockdown cells. Antibody (10 µg/mL) was treated for 24 h and then cell death was measured.